Published January, 2005

Frequency Dependence of the Complex Permittivity and Its Impact on Dielectric Sensor Calibration in Soils

T. J. Kelleners,* D. A. Robinson, P. J. Shouse, J. E. Ayars, and T. H. Skaggs

ABSTRACT

The capacitance (CAP) method and time domain reflectometry (TDR) are two popular electromagnetic techniques used to estimate soil water content. However, the frequency dependence of the real and imaginary part of the permittivity complicates sensor calibration. The frequency dependence can be particularly significant in fine-textured soils containing clay minerals. In this work, we applied both the CAP method and TDR to a nondispersive medium (fine sand) and a strongly dispersive medium (bentonite). The measurements were conducted for a range of water contents. Results using a network analyzer showed that the frequency dependence of the real permittivity of the bentonite was particularly strong below 500 MHz. Above this frequency, the real permittivity of the bentonite was mainly a function of the water content. The TDR predicted apparent permittivity in the bentonite was below the CAP predicted real permittivity at low water contents. This was attributed to the dispersive nature of the bentonite combined with the high frequency of operation of TDR (up to 3 GHz in dry soil). The CAP sensor (frequency of 100–150 MHz) overestimated the real permittivity of the bentonite at high water contents. An electric circuit model proved partially successful in correcting the CAP data by taking the dielectric losses into account. The TDR signal became attenuated at higher water contents. It seems worthwhile to raise the effective frequency of dielectric sensors above 500 MHz to benefit from the relatively stable permittivity region at this frequency.

Water content impacts crop growth directly, and also influences the fate of agricultural chemicals applied to soils. Estimation of soil water content, therefore, is important in agriculture (Dane and Topp, 2002, p. 417–1074). In the field, basically three methods are available: gravimetric techniques, nuclear techniques (e.g., neutron scattering), and electromagnetic techniques. Of these, electromagnetic techniques have become popular because they facilitate a rapid, safe, nondestructive, and easily automated estimation of soil water content.

Among the electromagnetic techniques, TDR is widely used in research (e.g., Topp et al., 1980; Heimovaara, 1994; Robinson et al., 2003). The ability to measure both water content and bulk electrical conductivity (EC) in the same soil volume contributes to the attractiveness of TDR. However, the emergence of low-cost, high-frequency oscillators has led to an increased interest in CAP techniques (e.g., Dean et al., 1987; Evett and Steiner, 1995; Paltineanu and Starr, 1997). Present-day CAP sensors are relatively inexpensive and easy to operate, and are becoming a popular choice for routine monitoring purposes.

Both TDR and CAP techniques measure soil water content indirectly. Both techniques actually respond to the permittivity of the soil. The relationship between the permittivity of the soil and the instrument output (travel time for TDR; resonant frequency for most CAP techniques) can be described with electric circuit theory. Examples of circuit theory applications can be found in Topp et al. (1980), Heimovaara (1994), and Lin (2003) for TDR and in Dean (1994), Robinson et al. (1998), and Kelleners et al. (2004a) for CAP techniques. The relationship between permittivity and soil water content, on the other hand, can be described separately using physical dielectric mixing models (e.g., Birchak et al., 1974; Dobson et al., 1985; Friedman, 1998) or empirical models (e.g., Topp et al., 1980; Malicki et al., 1996).

The interpretation of electromagnetic measurements is relatively straightforward if the soil is nonconductive and if all water molecules in the soil rotate freely as a function of the applied electromagnetic field. This is the case in sandy soils wetted with deionized water for frequencies below 17 GHz (the relaxation frequency of free water). The interpretation of electromagnetic measurements in saline soils and in fine-textured soils is more complicated. Ionic conductivity and clay-water-ion interactions may affect the permittivity reading. The significance of these processes is generally a function of the measurement frequency. Hence, permittivity may be both a function of water content and of frequency. Different frequencies propagate through a medium at different velocities if the permittivity of the medium changes with frequency. Such a medium is called a dispersive dielectric medium (Von Hippel, 1954a; Kraus, 1984).

In this work we will investigate the effect of the frequency dependence of permittivity on the estimation of soil water content with TDR and the CAP technique. The effect of ionic conductivity will be discussed as well. Experimental data are collected in the laboratory for a nondispersive medium (fine sand) and a strongly dispersive medium (bentonite). The frequency-dependence of the permittivity of most natural soils will be somewhere between these two extremes. The results therefore serve as bounds for most routine measurement work. The specific objectives of this study are (i) to quantify the

T.J. Kelleners and D.A. Robinson, Dep. of Plants, Soils, and Biometeorology, Utah State Univ., Logan, UT 84322; P.J. Shouse and T.H. Skaggs, USDA-ARS, George E. Brown, Jr. Salinity Lab., 450 W. Big Springs Road, Riverside, CA 92507; J.E. Ayars, USDA-ARS, Water Management Research Lab., 9611 S. Riverbend Ave., Parlier, CA 93648. This research was conducted at the George E. Brown, Jr. Salinity Laboratory, USDA-ARS, Riverside, CA. The mention of trade or manufacturer names is made for information only and does not imply an endorsement, recommendation, or exclusion by the USDA-ARS. Received 6 May 2004. *Corresponding author (tkelleners@cc.usu.edu).

Published in Soil Sci. Soc. Am. J. 69:67–76 (2005).

677 S. Segoe Rd., Madison, WI 53711 USA

Abbreviations: CAP, capacitance; EC, electrical conductivity; SF, scaled frequency; TDR, time domain reflectometry.

frequency-dependence of the complex permittivity of bentonite, (ii) to demonstrate the impact of dispersion and ionic conductivity on the water content–permittivity relationship as measured by TDR and the CAP technique, (iii) to evaluate correction procedures for obtaining the real permittivity from sensor data, and (iv) to comment on the optimum frequency of operation for dielectric sensors.

THEORY

The relative permittivity of a medium can be represented by a complex quantity ε_r^* (−) that has a real part ε_r' (−) describing energy storage, and an imaginary part ε_r'' (−) describing energy losses. The value of the permittivity varies as a function of the frequency of the applied electromagnetic field:

$$\varepsilon_r^*(\omega) = \varepsilon_r'(\omega) - j\varepsilon_r''(\omega) \quad [1]$$

where $j^2 = -1$ and ω (T^{-1}) is the angular frequency ($= 2\pi F$, with F [T^{-1}] being the frequency expressed in hertz). The imaginary part ε_r'' is the sum of a conductivity term and a relaxation term (Kraus, 1984):

$$\varepsilon_r''(\omega) = \sigma/(\omega\varepsilon_0) + \varepsilon_{r,rel}''(\omega) \quad [2]$$

where σ is the ionic conductivity ($L^{-3}\ T^3\ M^{-1}\ I^2$), expressed in S m^{-1}, ε_0 is the permittivity in vacuum ($L^{-3}\ T^4\ M^{-1}\ I^2$) ($= 8.8542 \times 10^{-12}$ F m^{-1}), and $\varepsilon_{r,rel}''$ is the loss (−) due to dielectric relaxation.

Time Domain Reflectometry

Time domain reflectometry measures the travel time of a step voltage pulse along a transmission line. In soil science applications, the transmission line generally consists of two or more metal rods embedded in the soil. The travel time of the voltage pulse can be related to apparent relative permittivity ε_a (−) through (Topp et al., 1980):

$$\varepsilon_a = (c/v)^2 = (ct/L)^2 = (\varepsilon_r'/2)[1 + (1 + \tan^2\delta)^{1/2}] \quad [3]$$

where c ($L\ T^{-1}$) is the velocity of light in vacuum ($= 2.9979 \times 10^8$ m s^{-1}), v ($L\ T^{-1}$) is the propagation velocity of the voltage pulse in the transmission line, t is the time (T), L is the length of the travel path of the voltage pulse (L), and tan δ is the loss tangent (−) defined as the ratio of the imaginary to the real permittivity, $\varepsilon_r''/\varepsilon_r'$. Note that Eq. [3] was derived by Von Hippel (1954a) for a single sinusoidal wave. The validity of this equation for a voltage pulse has yet to be proven (Hilhorst, 1998).

If $\tan\delta << 1$, Eq. [3] simplifies to:

$$\varepsilon_a = (c/v)^2 = (ct/L)^2 \approx \varepsilon_r' \quad [4]$$

which is commonly used in soil science applications (e.g., Noborio, 2001; Jones et al., 2002).

Capacitance Technique

The permittivity of the soil can also be determined by measuring the soil CAP:

$$C = g\varepsilon_r'\ \varepsilon_0 \quad [5]$$

where C is the capacitance ($L^{-2}\ T^4\ M^{-1}\ I^2$) expressed in farad, and g is a geometric factor (L) associated with the electrode configuration and the shape of the electromagnetic field penetrating the medium.

A method of measuring the CAP of the soil is to incorporate the soil into an oscillator circuit and measure the resonant frequency F:

$$F = 1/(2\pi\sqrt{L_tC_t}) \quad [6]$$

where L_t is the total circuit inductance ($L^2\ T^{-2}\ M\ I^{-2}$), expressed in henry, and C_t is the total circuit CAP.

The total circuit CAP for the CAP sensors used in this study is made up of three components, which act both in parallel and in series (Kelleners et al., 2004a):

$$C_t = C_s + C_pC_m/(C_p + C_m) \quad [7]$$

where C_m ($= g_m\varepsilon_{r,m}'\varepsilon_0$) is the capacitance of the medium, C_p ($= g_p\varepsilon_{r,p}'\varepsilon_0$) is the capacitance of the plastic access tube surrounding the sensor, and C_s is the capacitance due to stray electric fields. The subscript m denotes the medium and the subscript p denotes the plastic access tube.

Inserting Eq. [7] into Eq. [6] results in:

$$F = 1/\{2\pi\sqrt{L_t[C_s + C_pC_m/(C_p + C_m)]}\} \quad [8]$$

Equation [8] is valid for pure dielectrics (imaginary part of the permittivity is zero). For nonzero imaginary permittivity, the sum of the losses due to ionic conductivity and dielectric relaxation can be written as:

$$G = g_m\omega\varepsilon_r''\varepsilon_0 = g_m\sigma + g_m\omega\varepsilon_{r,rel}''\varepsilon_0 \quad [9]$$

where G ($L^{-2}\ T^3\ M^{-1}\ I^2$) is the sum of the dielectric losses, expressed in Siemens.

Equation [9] can be incorporated into an expression that describes the resonant frequency of the CAP sensors in media with dielectric losses. The procedure is explained in Kelleners et al. (2004a) and is not repeated here. The resulting equation reads:

$$\omega^2C_A^2 + G^2 - \omega^4C_sL_tC_A^2 - \omega^2C_sL_tG^2 - \omega^4L_tC_pC_mC_A - \omega^2L_tC_pG^2 = 0 \quad [10]$$

where $C_A = C_p + C_m$. Equation [10] can be solved for the angular frequency ω and for the medium capacitance C_m using the quadratic formula. The solutions are given in Kelleners et al. (2004a).

Water Content–Permittivity Relationship

Several physical and empirical models exist to relate the permittivity to the volumetric water content θ (−). The empirical equation of Topp et al. (1980) is generally applicable to coarse grained mineral soils:

$$\theta = -5.3 \times 10^{-2} + 2.92 \times 10^{-2}\varepsilon_a - 5.5 \times 10^{-4}\varepsilon_a^2 + 4.3 \times 10^{-6}\varepsilon_a^3 \quad [11]$$

Equation [11] is an empirical relationship that should only be used in the water content range of 0 to 0.55 for which it was intended. To also cover $\theta > 0.55$, a semitheoretical linear relationship may be used (e.g., Ledieu et al., 1986; Herkelrath et al., 1991; Heimovaara, 1993):

$$\theta = a\sqrt{\varepsilon_a} + b \quad [12]$$

The coefficients $a = 0.145$ and $b = -0.305$ in this so-called refractive index model can be obtained by minimizing the sum of squared differences between the predicted permittivity and the permittivity according to Eq. [11] using $\varepsilon_a(\theta)$ for $0 \le \theta \le 0.55$ and Topp's constraining point ($\theta = 1$; $\varepsilon_a = 81.5$).

MATERIALS AND METHODS

The dielectric sensor measurements were conducted in a laboratory using two distinctly different soil materials. Fine quartz sand was selected to represent a soil with no dielectric dispersion, while bentonite was chosen to represent a soil in which dielectric dispersion is severe. The experiments were performed in a 22-L plastic bucket (height = 36 cm, average i.d. = 28 cm), with an access tube located in the center (51-mm i.d., running through the bottom of the bucket). The water content ranged from dry soil to saturation for the sand and from dry soil to infinite dilution (pure water) for the bentonite. The soils were wetted to the desired water content by spraying with deionized water while stirring the soil in a trough. Care was taken to pack the soil in the bucket to a homogeneous bulk density and to a constant volume of 17.82 dm^3. The exact volumetric water content and dry bulk density of the packed soil were determined by weighing the filled bucket and by determining the wetness of the soil (= gravimetric water content) from a 30-cm^3 subsample taken from the trough. In all calculations it was assumed that the density of the solid phase was 2.65 g cm^{-3}.

Capacitance measurements were conducted with an EnviroSCAN probe (Sentek Pty Ltd., Kent Town, South Australia). The probe may hold up to 15 sensors and is designed to operate inside a polyvinyl chloride access tube. Each sensor consists of two brass rings (50.5-mm diam. and 25 mm high) mounted on a plastic sensor body and separated by a 12-mm plastic ring. The rings of the sensor form the plates of the capacitor (for details see Paltineanu and Starr, 1997). The sensor output is the resonant frequency (100–150 MHz). In this study, 12 sensors were read by moving the sensors one by one into the center of the access tube in the bucket. The sensor constants in Eq. [10] were determined with the simplified procedure of Kelleners et al. (2004a). In brief, the simplified procedure fixed the sensor constants L_t at 9.38×10^{-8} H and g_m at 0.176 m. Subsequently, the two remaining sensor constants C_s and g_p ($= C_p\varepsilon'^{-1}_{r,p}\varepsilon_0^{-1}$, with $\varepsilon'_{r,p} = 3$ [e.g., Von Hippel, 1954b]) were calculated by solving Eq. [8] using sensor readings in air and deionized water.

The TDR measurements were conducted with a two-rod probe (16.5-cm rods with a diam. of 0.3 cm, spaced 1 cm apart) connected to a TDR cable tester (Model 1502B, Tektronix Inc., Beaverton, OR). The frequency range of the excitation voltage of the cable tester is roughly between 20 kHz and 3.0 GHz. Time domain reflectometry measurements were taken by pushing the probe vertically into the soil. Five replicate measurements were made for each sample. The travel time of the voltage pulse was determined from the TDR waveforms using the WinTDR software (Version 6.0, Or et al., 2003). After each TDR measurement, the resistance R across the rods was measured by connecting the probe to a LRC Bridge (Model 2400, Electro Scientific Industries Inc., Portland, OR). The resistance measurements were conducted at a frequency of 1 kHz. The bulk EC σ was calculated using $1/R = a\sigma + b$. The regression coefficients $a = 0.2541$ m and $b = 0.0014$ S were determined during a separate calibration experiment with KCl solutions ranging from 0.0294 to 0.459 S m^{-1}, covering the approximate σ range in the bentonite. Soil temperature was measured with a k-type thermometer (Model 630, B&K Precision Corp., Yorba Linda, CA) using a 16-cm probe inserted vertically into the soil.

The dielectric properties (ε'_r and ε''_r) of the bentonite were measured as a function of frequency with a network analyzer (Model 8753B, Hewlett-Packard, Palo Alto, CA) using a dielectric probe (Model 85070B, Hewlett-Packard) with a 3.17-cm^3 sample holder. Network analyzers measure the reflection and transmission characteristics of a medium with a broad bandwidth signal (frequencies between 300 KHz and 3 GHz). The sample holder was packed to as many as four different bulk densities for each soil wetness. Interpolation was used to determine ε'_r and ε''_r for the bulk density of the bentonite in the 22-L bucket. Each dielectric measurement was followed by a resistance measurement using the LRC bridge connected to 0.08 and 0.02 cm^2 vertical plates on opposite sides of the sample holder. Bulk EC was calculated using $1/R = 2.19 \times 10^{-4}\sigma + 2.46 \times 10^{-6}$ (regression coefficients determined during a separate calibration experiment with KCl solutions of 0.002–0.474 S m^{-1}). The soil temperature was measured with the k-type thermometer using a 2-mm probe, which was inserted vertically into the sample holder. The dielectric properties of the sand were not measured, as previous work had shown them to be frequency-independent.

RESULTS AND DISCUSSION

Dielectric Properties of Bentonite

The network analyzer data for bentonite are summarized in Fig. 1. Real and imaginary permittivity are given as a function of frequency for seven different water contents. The seven curves were carefully selected from a larger data set to represent a wide range of water contents while limiting the variations in density (dry bulk density values for the selected curves are between 0.936 and 1.097 g cm^{-3}). The dielectric losses due to ionic conductivity and dielectric relaxation are also given. The losses due to relaxation were calculated by subtracting $\sigma\omega^{-1}\varepsilon_0^{-1}$ from ε''_r (see Eq. [2]).

In nondispersive media, ε'_r only changes as a function of θ. Figure 1a shows that ε'_r for bentonite also changes with frequency. The higher the frequency, the lower the value of ε'_r. The change of ε'_r with frequency is the result of complex clay–water–ion interactions. Reductions in ε'_r may be due to decreased polarizability of the water molecules because of the presence of clay surfaces and ions. Increases in ε'_r that are in excess of what might be expected on the basis of water content alone may also occur. Figure 1a, for example, shows that the value of ε'_r may become as high as 100 at low frequencies (maximum $\varepsilon'_r = 341$ for $\theta = 0.594$ at $F = 10$ MHz, value not shown). Such high values for ε'_r cannot be explained by considering the soil as a simple mixture of solids (ε'_r = 3–8), air ($\varepsilon'_r = 1$), and water ($\varepsilon'_r \approx 80$).

The ε'_r value of free water at room temperature and under atmospheric pressure does not exceed 80, regardless of the frequency. So, the polarization of the water molecules alone cannot explain $\varepsilon'_r > 80$ in the bentonite at low frequencies. Additional energy may be stored in the bentonite by the polarization of the diffuse electrical double layer of the clay particles: the cations in the double layer may move around the clay particles with the changes in the electric field, thus creating a large effective dipole (Hasted, 1973). Additional energy can also be stored in the soil through the Maxwell–Wagner effect: ions in the soil water may not be able to move freely with the electric field due to the presence of the clay surfaces. The resulting accumulation of charge at the surfaces increases the polarizability of the soil, especially at low frequencies (Sihvola, 1999). Increases in

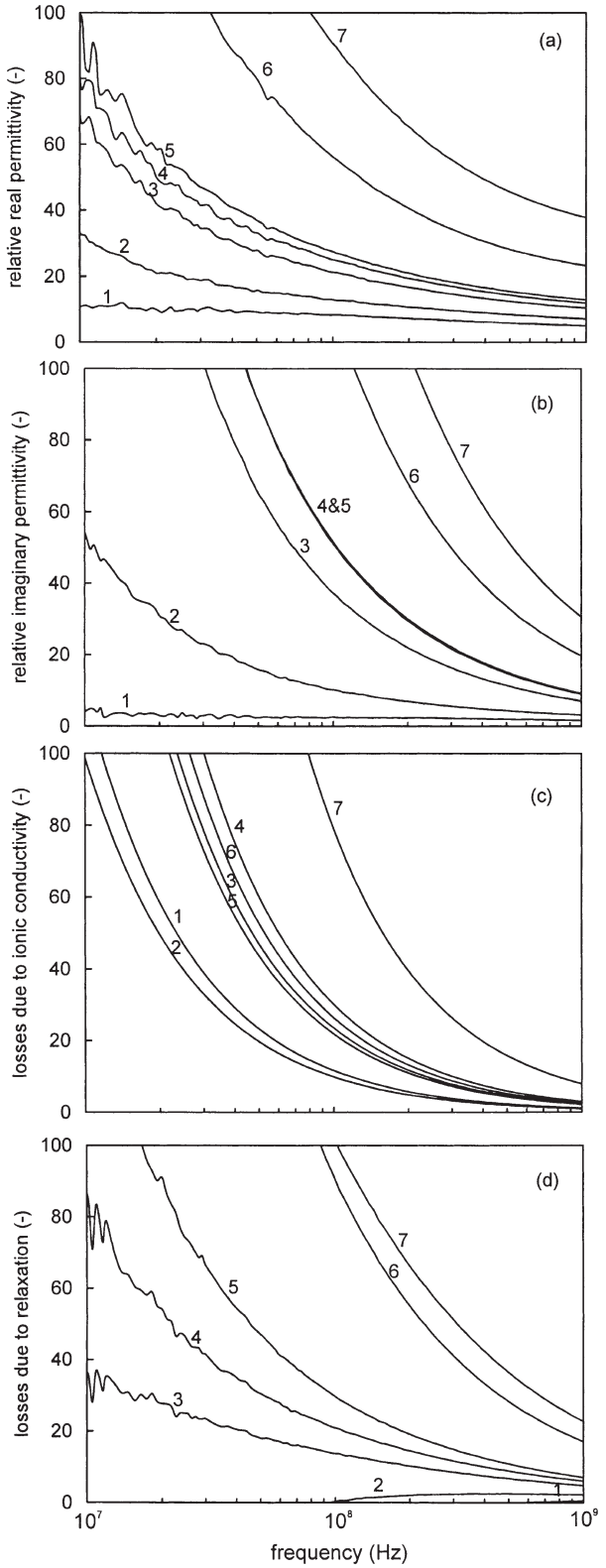

Fig. 1. (a) Real and (b) imaginary permittivity in bentonite as a function of frequency. Results are from the network analyzer for different volumetric water contents (1 = 0.088; 2 = 0.190; 3 = 0.292; 4 = 0.326; 5 = 0.413; 6 = 0.521; 7 = 0.594). Losses due to ionic conductivity $\sigma\omega^{-1}\varepsilon_0^{-1}$ (c) were computed from resistance measurements with a LRC bridge. Losses due to relaxation (d) were calculated by subtracting $\sigma\omega^{-1}\varepsilon_0^{-1}$ from ε_r''. Frequency values on the *x* axis are on log scale.

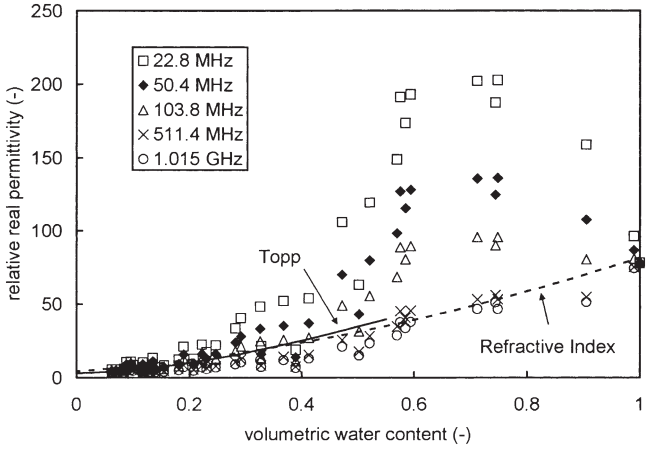

Fig. 2. Real permittivity as a function of water content for bentonite. Results are from the network analyzer for five different frequencies. The $\varepsilon_a(\theta)$ relationships according to Topp and the refractive index model are also shown.

ε_r' of up to 100 (clay with $\theta = 0.5$ at 1 MHz) and 140 (Beaumont clay [fine, smectitic, hyperthermic Chromic Dystraquerts] with wetness = 0.39 at 50 MHz) have been found by others in clays (Campbell, 1990; Saarenketo, 1998). Extraordinary large ε_r' values in bentonite at low frequencies have also been reported by Logsdon and Laird (2002).

Figure 1b shows that ε_r'' is also a function of both water content and the measurement frequency in the bentonite. The highest dielectric losses occur at high water contents and at low frequencies. The dielectric losses due to ionic conductivity decrease with frequency according to $\sigma\omega^{-1}\varepsilon_0^{-1}$ (Fig. 1c). The higher the frequency, the less energy is lost moving the ions around in the soil water. The relative contribution of ionic conductivity and relaxation to the dielectric losses should not be inferred from Fig. 1c and 1d. First, the relaxation losses have not been measured independently. Second, ε_r'' (Fig. 1b) and the losses due to ionic conductivity (1c) are not completely in agreement. For example, Fig. 1b indicates that the dielectric losses for $\theta = 0.088$ are small across the complete frequency range. In contrast, Fig. 1c shows that the losses at this water content may be as high as 100 at low frequencies. This apparent discrepancy is caused by the different measurement techniques that were used (network analyzer for ε_r'', LRC bridge for σ).

The network analyzer data can also be used to show ε_r' as a function of water content for different frequencies (Fig. 2). Note that the $\varepsilon_r'(\theta)$ data do not generally follow a smooth curve because of differences in bulk density between points. The equation of Topp et al. (1980) (Eq. [11]) and the refractive index model (Eq. [12]) are given for comparison. Figure 2 shows that the $\varepsilon_r'(\theta)$ data for bentonite only agree with the $\varepsilon_a(\theta)$ curves for measurement frequencies of 500 MHz or higher. Below 500 MHz, the relationship between ε_r' and θ strongly changes as a function of frequency. This indicates that bentonite behaves the same at high frequencies as mineral soils that do not show a frequency dependence (including sands).

This important observation can be interpreted in two

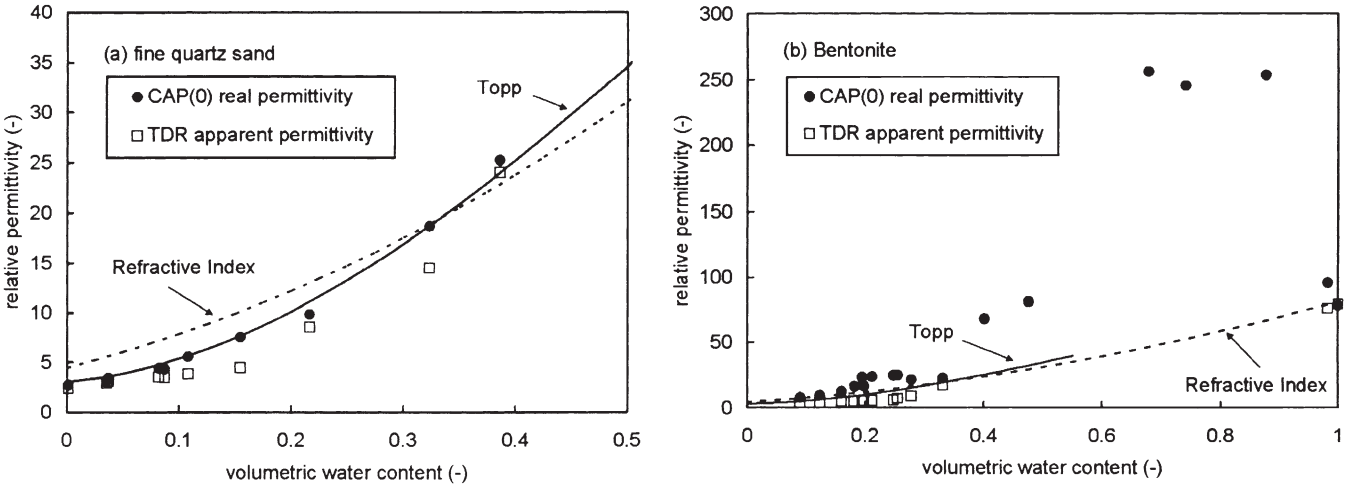

Fig. 3. Real and apparent permittivity as a function of water content for (a) fine quartz sand and (b) bentonite. Results are for the uncorrected capacitance sensor and TDR. Values for the TDR in bentonite for $0.401 \leq \theta \leq 0.877$ are missing due to signal attenuation.

different ways. One might conclude that the Maxwell–Wagner effect and the double-layer dipole effect, which increase ε_r', and reductions in the polarizability of the water molecules, which decrease ε_r', cancel each other out above 500 MHz. Such a coincidence seems unlikely. On the other hand, one might also conclude that none of these processes are significant at high frequencies and can therefore be ignored. This would be surprising since reductions in ε_r' due to clay–water bonding should be significant in bentonite. Both explanations are therefore not completely satisfying. More information, probably including different clay-like materials, is needed to resolve this issue.

Uncorrected Capacitance and Time Domain Reflectometry Data

Calculated permittivity in the bucket according to the CAP data and the TDR data is shown as a function of water content in Fig. 3a (fine quartz sand) and 3b (bentonite). Note that the CAP data refer to ε_r' while the TDR data refer to ε_a. The CAP data are only for one of the sensors ($C_s = 10.58 \times 10^{-12}$ F; $g_p = 0.626$ m). The results for the 11 other sensors were practically the same and are therefore not shown. The CAP-ε_r' values were calculated using Eq. [5] and [8] with the assumption that the dielectric losses are zero, hence the denotation CAP(0) in Fig. 3a and 3b. As we will see, the assumption of zero dielectric losses is reasonable for the sand, but not for the bentonite. The TDR-ε_a values are the average of five replicates. Coefficients of variation for the TDR-ε_a values at specific water contents varied between 0.9 and 5.6% for the fine sand and between 0 and 7.3% for the bentonite.

Figure 3a shows that the CAP data for the sand compare well with Topp's curve, as would be expected. The TDR-ε_a values fall below this curve for $0.082 \leq \theta \leq 0.323$. The underestimation by TDR is probably due to the experimental procedure. The 16.5-cm vertically-inserted TDR rods covered only the upper part of the 36-cm deep bucket and measurements were made after the CAP readings. Redistribution of the soil water in the sand started immediately after packing, making the top part of the bucket relatively dry and the bottom part relatively wet. The CAP readings were less affected by redistribution because they were measured first, and because the CAP sensor was positioned in the middle of the bucket. At complete saturation ($\theta = 0.386$), where redistribution does not occur, the TDR-ε_a value is in agreement with Topp's curve.

The CAP and TDR data for bentonite agree reasonably well with Topp's curve at low water content (Fig. 3b). The CAP-ε_r' values are higher than the TDR-ε_a values. Given that $\varepsilon_a(F) \geq \varepsilon_r'(F)$ (Eq. [3]), and assuming that CAP-$F <$ TDR-F, this suggests that the bentonite is dispersive even at the low water contents. Some of the variability in ε_r' and ε_a within the CAP and TDR data sets is due to differences in bulk density. The CAP data for $0.401 \leq \theta \leq 0.877$ are clearly higher than the predicted values. These relatively high ε_r' values may be due to additional polarization in the bentonite, or due to the neglect of the dielectric losses, or a combination of these. Note that all TDR readings are missing for $0.401 \leq \theta \leq 0.877$. This is due to the high dielectric losses. At high G, the voltage pulse may become completely attenuated before it is reflected back to the cable tester. At $\theta \geq 0.877$, the CAP technique and TDR give ε_r' and ε_a values close to that of free water ($\varepsilon_r' \approx 80$), indicating that additional polarization has ceased and that dielectric losses have decreased.

Corrected Capacitance Data

The dielectric losses for the CAP readings in the bentonite are shown in Fig. 4. The results are for the same sensor as selected previously. The total dielectric losses $G = g_m \omega \varepsilon_r'' \varepsilon_0$ were estimated from the imaginary permittivity $\varepsilon_r''(\omega)$ of the network analyzer (interpolated for the correct bulk density) using the angular frequency of the CAP sensor. The dielectric losses due to ionic conductivity were calculated in two different ways using $G(\text{cond}) = g_m \sigma$. First, with σ derived from the resistance measurements in the bucket (Fig. 4a), and second, with σ derived from the resistance measurements in the di-

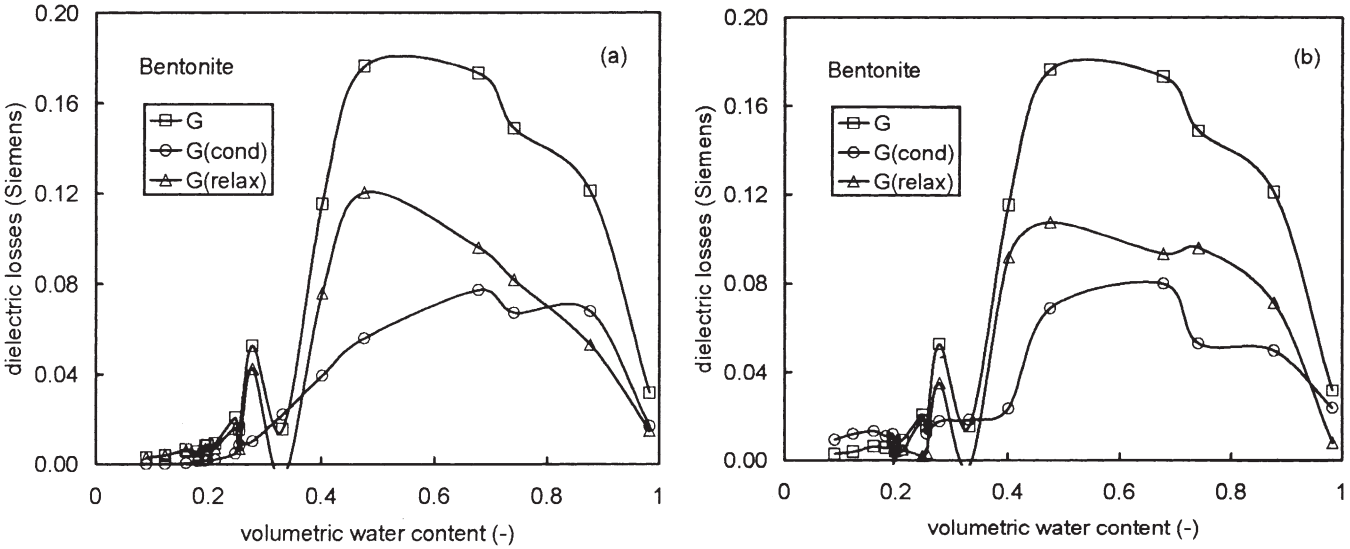

Fig. 4. Dielectric losses (G) as a function of water content. Losses due to ionic conductivity were calculated from the resistance measurements in (a) the bucket and (b) the dielectric sample, respectively. The bulk electrical conductivity (EC) of the dielectric sample was corrected for temperature differences between the sample and the bucket using $EC_b = EC_s - 0.02EC_s(T_s - T_b)$, where the subscripts b and s stand for bucket and sample, respectively, and T is the temperature in degrees Celsius.

electric sample (Fig. 4b). The dielectric losses due to relaxation were calculated from $G(\text{relax}) = G\text{-}G(\text{cond})$. Figure 4 shows that the total dielectric losses are low for $\theta \leq 0.211$ and high for $0.401 \leq \theta \leq 0.877$. Some fluctuations in the G values occur for $0.247 \leq \theta \leq 0.331$. This may be due to the presence of a percolation threshold around this water content. The conducting water becomes connected at this threshold, replacing air as the continuous phase in the soil. This alteration of the solid, water, and air phase configuration can cause a sudden change in the dielectric properties of the bentonite (e.g., Friedman, 1998). Figures 4a and 4b show that losses due to both ionic conductivity and dielectric relaxation play a role in the bentonite in the frequency range of the CAP sensor (100–150 MHz). Note that the highest σ value was 4.5 dS m^{-1} for $\theta = 0.678$.

The CAP data for bentonite are studied in detail in Fig. 5. The sensor frequency F is converted to the real permittivity ε_r' in four different ways for each water content: (i) ε_r' is calculated from Eq. [5] and [8] (dielectric losses neglected), denoted as CAP(0); (ii) ε_r' is calculated from Eq. [5] and [10] with $G = g_m\omega\varepsilon_r''\varepsilon_0$ (all dielectric losses accounted for), denoted as CAP(G); (iii) ε_r' is calculated from Eq. [5] and [10] with $G(\text{cond}) = g_m\sigma$ (relaxation losses neglected), with σ calculated from the resistance measurements in the dielectric sample, denoted as CAP(R_s); and (iv) ε_r' is calculated from Eq. [5] and [10] with $G(\text{cond}) = g_m\sigma$ (again, relaxation losses neglected), with σ calculated from the resistance measurements in the bucket, denoted as CAP(R_b). The value of $\varepsilon_r'(F)$ as measured with the network analyzer, and as interpolated for the correct bulk density value, is also given. Because Eq. [10] is quadratic, the CAP circuit-model may give two values for ε_r' at certain water contents. It is impossible to tell for sure which of the two values is correct (for details see Kelleners et al., 2004a).

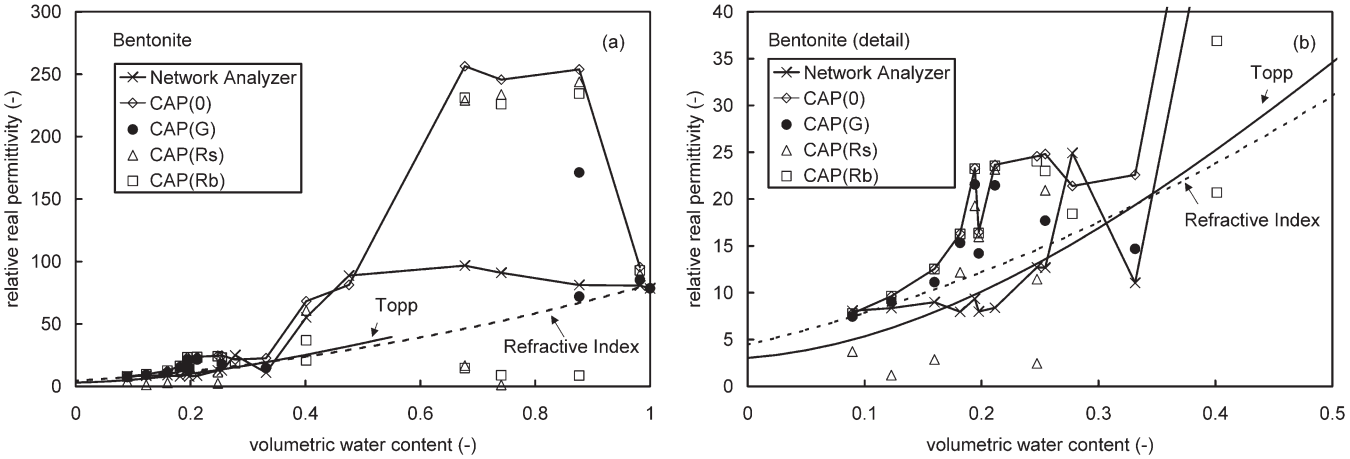

Fig. 5. Real permittivity as a function of water content for bentonite. Results are from the network analyzer and the capacitance sensor. The comments between parentheses stand for uncorrected data (0), data corrected for the total dielectric losses (G), data corrected for the ionic conductivity as derived from the resistance measured in the sample (Rs), and data corrected for the ionic conductivity as derived from the resistance measured in the bucket (Rb). Plot (b) is a close-up of plot (a).

First we compare the uncorrected CAP(0) data with the ε_r' values from the network analyzer, which serve as a reference. Figure 5 shows that at $\theta = 0.090$ both techniques indicate $\varepsilon_r' = 7.5$. For $0.090 < \theta \leq 0.255$, the ε_r' values for CAP(0) exceed those from the network analyzer. This is unexpected because the dielectric losses are low at these water contents. Also, there should be no differences in ε_r' (the measurement frequencies are the same). The different ε_r' values could be due to differences in bulk density. For $\theta > 0.331$, both techniques show an increase in ε_r' that far exceeds Topp's curve. This increase is probably due to an increase in the real permittivity brought about by the crossing of the percolation threshold. At $\theta > 0.476$, the CAP(0)-ε_r' and the network analyzer-ε_r' start to deviate significantly. This can be attributed to the high dielectric losses at these water contents which affect the CAP(0) data. For $\theta \geq 0.982$, the dielectric losses and the increases in the real permittivity are no longer apparent, and both techniques fall back to an ε_r' value of around 80 (the permittivity of pure water).

We now compare CAP(G), CAP(R_s), and CAP(R_b). Ideally, CAP(R_s)-ε_r' values should be equal to CAP(R_b)-ε_r' values. This is not the case for the low water contents where the CAP(R_s)-ε_r' values seem to be underestimated due to an overestimation of the ionic conductivity (see also Fig. 4b). However, at higher water contents, the comparison between CAP(R_s) and CAP(R_b) is reasonable. Accounting solely for the losses due to ionic conductivity, which can be measured relatively easily, is clearly not enough to arrive at reasonable estimates of ε_r' at high water contents. Incorporation of the relaxation losses seems essential, although there are not enough CAP(G) data points in Fig. 5 to prove this. In practice, the losses due to relaxation will be difficult to quantify, as there is no straightforward method available to separate relaxation and ionic conductivity directly. Note that for $0.401 \leq \theta \leq 0.741$, no solutions were obtained for CAP(G). At these water contents, the high dielectric losses result in the sensor frequency being insensitive to $\varepsilon_r'(\theta)$. Or in other words, at high G, the dielectric losses are completely overshadowing the effect of the real permittivity on the sensor frequency (Kelleners et al., 2004a).

It is interesting to note that the increase in the dielectric losses G (Fig. 4) and the increase in the real permittivity ε_r' (Fig. 5) occur more or less simultaneously when θ increases from 0.331 to 0.401. A similar observation was made by Campbell (1990) while studying the dielectric properties of soils with frequencies varying from 1 to 50 MHz. It is likely that there is a percolation threshold around this water content that depends on the bulk density. It was mentioned earlier that the phase configuration of the soil changes at this percolation threshold because the conducting water phase becomes connected. This contributes both to the real permittivity and to the ionic conductivity (and hence to the dielectric losses). Whether the real permittivity increases also through double-layer polarizability and the Maxwell-Wagner effect, or other additional energy storage processes, is not known.

Assessment of the Time Domain Reflectometry Data

With TDR, the voltage pulse is made up of a wide range of frequencies. The lowest frequencies are determined by the pulse width of the TDR signal, which is 25 μs. This corresponds to a minimum frequency of about 20 kHz (Heimovaara, 1994). The maximum frequency in the TDR input signal can be estimated from the rise time t_r (T) of the voltage pulse, where rise time is defined as the time required for the voltage to rise from 10% of its asymptotic value to 90% of its asymptotic value. The corresponding maximum frequency F_m (T^{-1}) can be calculated as (e.g., Bogart et al., 2004)

$$F_m = \ln(0.9/0.1)/2\pi t_r \quad [13]$$

This equation is used in electrical engineering to describe the frequency characteristics of a low-pass filter. It is only accurate when the energy contained in the voltage pulse is equally distributed across the frequency bandwidth and in the absence of significant dispersion (e.g., Hook et al., 2004). Equation [13] results in $F_m = 1.75$ GHz with $t_r = 200$ ps for the 1502B cable tester. The F_m value of 1.75 GHz strictly refers to the TDR input signal. The highest frequencies in the reflected signal depend on the probe length, probe construction quality, connector quality, and the dielectric properties of the soil. The longer the probe, and the higher the permittivity, the more the higher frequencies are filtered out.

We used Eq. [13] to approximate F_m values for the reflected TDR signals in the bentonite by determining the rise time t_r of the reflection at the end of the probe. The resulting F_m values should be handled with care because most energy in the voltage pulse of the TDR is contained in the lower frequencies and because of the dispersion in the bentonite which will be especially significant at the higher water contents. For comparison, we also calculated F_m from the network analyzer data by converting $\varepsilon_r'(\omega)$ and $\varepsilon_r''(\omega)$ into $\varepsilon_a(\omega)$ (Eq. [3]), and by subsequently determining the frequency for which $\varepsilon_a(\omega)$ equals the TDR-ε_a. The resulting F_m values are shown in Table 1 as a function of θ, dry bulk density, and the TDR-ε_a for the bentonite in the bucket. Note that the TDR-ε_a values are associated with the highest frequencies in the reflected signal because the waveform analysis uses the first reflection at the end of the probe to find the travel time t (Heimovaara et al., 1996).

Table 1 shows that for $0.090 \leq \theta \leq 0.211$ F_m decreases as the permittivity increases. As mentioned earlier, the higher the permittivity, the more the higher frequencies are filtered out. The F_m values calculated from the network analyzer data at the low water contents are significantly higher than the F_m values obtained from the rise time method. Some of the F_m values in the last column even exceed the bandwidth of the network analyzer which goes from 300 KHz to 3 GHz. Maximum frequencies in excess of 3 GHz for the 1502B cable tester were reported earlier by Heimovaara et al. (1996) based on a frequency domain analysis of the TDR signal in air.

Table 1. Calculated maximum frequency (F_m) of the reflected TDR signal for the bentonite in the bucket using a rise time method (Eq. [13]) and using the network analyzer data.

θ	Dry bulk density	ε_a	F_m Eq. [13]	F_m Netw. An.
	g cm^{-3}		MHz	
0.090	0.953	3.6	447.3	>3000
0.123	0.872	4.3	382.0	>3000
0.160	0.830	5.0	302.5	2006.9
0.182	0.766	5.0	297.1	1194.3
0.194	0.819	5.7	270.6	1158.4
0.198	0.695	5.0	271.8	978.7
0.211	0.743	5.5	260.0	763.0
0.247	0.716	6.1	266.8	2729.2
0.255	0.676	7.3	310.1	>3000
0.278	0.615	8.9	369.5	>3000
0.331	0.656	17.4	1107.4	81.1
0.401	0.721	–†	–	–
0.476	0.815	–	–	–
0.678	0.656	–	–	–
0.741	0.537	–	–	–
0.877	0.353	–	–	–
0.982	0.042	76.2	322.6	346.7
1.000	0.000	79.5	486.3	<0.3

† TDR data for $0.401 \leq \theta \leq 0.877$ could not be analyzed due to complete attenuation of the voltage pulse.

The above indicates that the rise time method (Eq. [13]) underestimates F_m.

The F_m estimates for $0.247 \leq \theta \leq 0.331$ in Table 1 are inconsistent and should be discarded. The rise time F_m calculation is invalidated because of dielectric dispersion and because of TDR signal attenuation due to dielectric losses at these water contents. The network analyzer F_m calculation suffers from the fact that interpolation is used to obtain $\varepsilon_r'(\omega)$ and $\varepsilon_r''(\omega)$ for the dry bulk density in the bucket. Small differences in the phase configuration of the bentonite may result in large differences in $\varepsilon_r'(\omega)$ and $\varepsilon_r''(\omega)$ because of the proximity of the percolation threshold at $0.247 \leq \theta \leq 0.331$. In contrast, the F_m values for $0.982 \leq \theta \leq 1.000$ for the rise time method appear reasonable. Dielectric losses and dielectric dispersion are no longer a significant factor at these high water contents. The F_m value of < 0.3 MHz calculated from the network analyzer data at $\theta = 1.0$ is not correct. The TDR-ε_a value was completely outside the range of network analyzer $\varepsilon_a(\omega)$ values, probably because of differences in temperature.

Capacitance Sensors in Soil

Conventionally, CAP data are calibrated by plotting the volumetric water content against the scaled frequency, SF (−) (e.g., Paltineanu and Starr, 1997):

$$SF = (F_a - F_s)/(F_a - F_w) \quad [14]$$

where F_a is the sensor frequency (T^{-1}) in air, F_s is the sensor frequency in soil, and F_w is the sensor frequency in deionized water.

Figure 6 shows the SF-θ relationship for the sand and the bentonite. Earlier results for a saline silty clay soil from the west side of California's San Joaquin Valley are also given. These CAP measurements were taken in situ at depths of 4.5 to 116.5 cm below the soil surface (Kelleners et al., 2004b). The two SF(θ) curves in Fig. 6 were calculated by combining the respective $\varepsilon_a(\theta)$ relationships with the theoretical frequency response in nonlossy media (Eq. [8]). The data for the fine sand are in excellent agreement with Topp's equation, as expected. The fine sand exhibits no dispersion and the ionic conductivity is negligible. These are ideal properties for electromagnetic techniques.

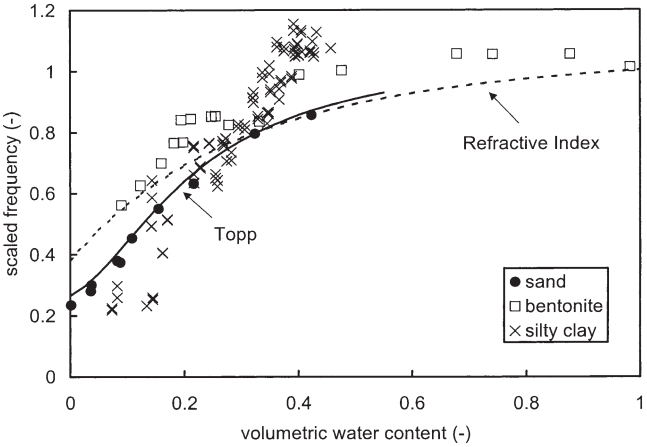

Fig. 6. Scaled frequency as a function of water content. Results for fine quartz sand, bentonite, and a saline silty clay soil. The curves were calculated by combining the respective $\varepsilon_a(\theta)$ relationships with the electric circuit model that assumes no dielectric losses (Eq. [8]).

The fits for the silty clay and bentonite data are less satisfactory. At $\theta < 0.2$, several of the silty clay data points show a relatively low SF. This is likely due to air gaps between the access tube and the dry topsoil (low θ values are all from the top 20 cm of the soil). For $0.211 \leq \theta \leq 0.278$, the SF values for bentonite are still higher than those for the silty clay. This suggests that the real permittivity in the bentonite is higher than the real permittivity in the silty clay. This could be due to the higher clay content for bentonite, which increases the possibility of additional polarization. For $\theta > 0.3$, the SF values for the silty clay exceed those for the bentonite and even become higher than 1. If $SF > 1$, then $F_s < F_w$ (Eq. [14]), which would be improbable in nondispersive, nonconductive soil. The high SF values for the silty clay are attributed to the high ionic conductivity in this saline soil (σ values up to 15.0 dS m^{-1}). Differences in the real permittivity between the bentonite and the silty clay could again also play a role.

Implications for Dielectric Sensor Design

The results of this study show that CAP measurements in fine textured soils are not straightforward. Present-day CAP sensors operate at a frequency of 150 MHz or lower where the frequency dependence of the real permittivity cannot be ignored. Dielectric losses due to ionic conductivity and relaxation also have a significant impact on the sensor frequency and need to be taken into account. The dielectric data from the network analyzer suggest that CAP measurements at 500 MHz or higher might improve the performance of the sensors. Between 500 MHz and 1 GHz, the real permittivity of the bentonite is almost frequency-independent, and mainly changes as a function of water content. This is a highly desirable feature. A higher frequency of operation would also reduce the dielectric

losses due to ionic conductivity ($= \sigma\omega^{-1}\varepsilon_0^{-1}$). Other fine-textured materials have to be examined to see whether they exhibit the same frequency behavior before more definitive design recommendations can be made.

The performance of TDR in the bentonite is more difficult to interpret. This is partly due to uncertainties about the frequency of operation. Results from Table 1 suggest that the TDR setup used in this study operates at frequencies > 3 GHz in dry soils and up to 763.0 MHz at $\theta = 0.211$. In any case, it can be concluded that the frequency of operation of the TDR was higher than that of the CAP technique. The TDR results were therefore less susceptible to dielectric dispersion and ionic conductivity. The use of shorter waveguides may have improved the performance of the TDR by reducing the attenuation of the higher frequencies. This reduction in attenuation would also have increased the effective water content range in the bentonite, which was now limited to $\theta \leq 0.331$ and $\theta \geq 0.982$.

CONCLUSIONS

The network analyzer data show that the dielectric properties of the bentonite are clearly frequency-dependent below 500 MHz. Above this frequency, the real permittivity becomes mainly a function of the soil water content. Topp's curve and the refractive index model described the water content–permittivity relationship for the bentonite fairly well for frequencies > 500 MHz, which was a surprise. We expected that additional polarizations in the bentonite due to double-layer dipoles and the Maxwell-Wagner effect, combined with reductions in the polarizability of the water molecules due to the presence of clay surfaces and ions, would result in a $\varepsilon_r'(\theta)$ relationship that differed from the relationship found for most mineral soils.

Capacitance and TDR readings in the fine sand confirmed that electric circuit theory combined with Topp's curve is able to describe the $\varepsilon_r'(\theta)$ relationship in this nondispersive and nonconductive material. In contrast, CAP readings in the bentonite resulted in permittivity values that exceeded Topp's curve. Increased permittivity due to additional polarization and dielectric losses due to ionic conductivity and dielectric relaxation were clearly nonnegligible in this case. Interpretation of the TDR readings in bentonite was incomplete because of signal attenuation associated with high dielectric losses at the higher water contents. At low water contents, the TDR-predicted ε_a values were consistently below the CAP predicted ε_r' values. This was attributed to the dispersive nature of the bentonite combined with the higher frequency of operation of TDR.

A comparison between the network analyzer data and the CAP data for the bentonite indicated that ε_r' increased for disproportionately $\theta > 0.331$. This coincided with an increase in the bulk EC around this water content. This suggested the presence of a percolation threshold. We speculated that the changes in the dielectric behavior were due to significant changes in the phase configuration and increased connectivity of the conducting fluid phase at $\theta > 0.331$. We also found that the dielectric losses for the CAP readings in bentonite were especially high for $0.401 \leq \theta \leq 0.877$. Losses due to both ionic conductivity and dielectric relaxation were found to be significant.

The maximum frequency in the reflected TDR signal was estimated from the rise time and from the network analyzer data. Calculated maximum frequencies from the rise time appeared to be too low. Calculated maximum frequencies from the network analyzer data ranged between 346.7 and > 3000 MHz, depending on the water content of the bentonite. The TDR frequencies were significantly higher than the operational frequency of the CAP sensors, which was 100 to 150 MHz. It seems worthwhile to try and raise the effective frequency of dielectric sensors above 500 MHz to benefit from the apparently stable permittivity region at this frequency. The frequency response of other clay-like materials should be tested before more definitive design recommendations can be made.

ACKNOWLEDGMENTS

David Robinson would like to acknowledge funding provided in part by USDA-NRI grant 2002-35107-12507.

REFERENCES

Birchak, J.R., C.G. Gardner, J.E. Hipp, and J.M. Victor. 1974. High dielectric constant microwave probes for sensing soil moisture. Proc. IEEE 62:93–98.

Bogart, T.F., J.S. Beasley, and G. Rico. 2004. Electronic devices and circuits. 6th ed. Prentice Hall, Columbus, OH.

Campbell, J.E. 1990. Dielectric properties and influence of conductivity in soils at one to fifty Megahertz. Soil Sci. Soc. Am. J. 54:332–341.

Dane, J.H., and G.C. Topp (ed.) 2002. Methods of soil analysis. Part 4—Physical methods. SSSA Book Ser. No. 5. SSSA, Madison, WI.

Dean, T.J. 1994. The IH capacitance probe for measurement of soil water content. Rep. No. 125. Institute of Hydrology, Wallingford, UK.

Dean, T.J., J.P. Bell, and A.J.B. Baty. 1987. Soil moisture measurement by an improved capacitance technique, part I. Sensor design and performance. J. Hydrol. (Amsterdam) 93:67–78.

Dobson, M.C., F.T. Ulaby, M.T. Hallikainen, and M.A. El-Rayes. 1985. Microwave dielectric behavior of wet soil. Part II: Dielectric mixing models. IEEE Trans. Geosci. Remote Sens. GE-23:35–46.

Evett, S.R., and J.L. Steiner. 1995. Precision of neutron scattering and capacitance type soil water content gauges from field calibration. Soil Sci. Soc. Am. J. 59:961–968.

Friedman, S.P. 1998. A saturation degree-dependent composite spheres model for describing the effective dielectric constant of unsaturated porous media. Water Resour. Res. 34:2949–2961.

Hasted, J.B. 1973. Aqueous dielectrics. Chapman and Hall, London.

Heimovaara, T.J. 1993. Design of triple-wire time domain reflectometry probes in practice and theory. Soil Sci. Soc. Am. J. 57:1410–1417.

Heimovaara, T.J. 1994. Frequency domain analysis of time domain reflectometry waveforms. 1. Measurement of the complex dielectric permittivity of soils. Water Resour. Res. 30:189–199.

Heimovaara, T.J., E.J.G. de Winter, W.K.P. van Loon, and D.C. Esveld. 1996. Frequency-dependent dielectric permittivity from 0 to 1 GHz: Time domain reflectometry measurements compared with frequency domain network analyzer measurements. Water Resour. Res. 32:3603–3610.

Herkelrath, W.N., S.P. Hamburg, and F. Murphy. 1991. Automatic, real-time monitoring of soil moisture in a remote field area with time domain reflectometry. Water Resour. Res. 27:857–864.

Hilhorst, M.A. 1998. Dielectric characterization of soil. Ph.D. diss. Wageningen Agric. Univ., Wageningen, the Netherlands.

Hook, W.R., T.P.A. Ferré, and N.J. Livingston. 2004. The effects of salinity on the accuracy and uncertainty of water content measurement. Soil Sci. Soc. Am. J. 68:47–56.

Jones, S.B., J.M. Wraith, and D. Or. 2002. Time domain reflectometry measurement principles and applications. Hydrol. Process. 16:141–153.

Kelleners, T.J., R.W.O. Soppe, D.A. Robinson, M.G. Schaap, J.E. Ayars, and T.H. Skaggs. 2004a. Calibration of capacitance probe sensors using electric circuit theory. Soil Sci. Soc. Am. J. 68:430–439.

Kelleners, T.J., R.W.O. Soppe, J.E. Ayars, and T.H. Skaggs. 2004b. Calibration of capacitance probe sensors in a saline silty clay soil. Soil Sci. Soc. Am. J. 68:770–778.

Kraus, J.D. 1984. Electromagnetics. 3rd ed. McGraw-Hill, New York.

Ledieu, J., P. de Ridder, P. de Clerck, and S. Dautrebande. 1986. A method of measuring soil moisture by time-domain reflectometry. J. Hydrol. (Amsterdam) 88:319–328.

Lin, C.-P. 2003. Frequency domain versus travel time analysis of TDR waveforms for soil moisture measurements. Soil Sci. Soc. Am. J. 67:720–729.

Logsdon, S.D., and D.A. Laird. 2002. Dielectric spectra of bound water in hydrated Ca-smectite. J. Non-Crystalline Solids 305:243–246.

Malicki, M.A., R. Plagge, and C.H. Roth. 1996. Improving the calibration of dielectric TDR soil moisture determination taking into account the solid soil. Eur. J. Soil Sci. 47:357–366.

Noborio, K. 2001. Measurement of soil water content and electrical conductivity by time domain reflectometry: A review. Comput. Electron. Agric. 31:213–237.

Or, D., S.B. Jones, J.R. Van Shaar, S. Humphries, and L. Koberstein. 2003. Users guide WinTDR. Version 6.0. Utah State Univ., Logan, UT.

Paltineanu, I.C., and J.L. Starr. 1997. Real-time soil water dynamics using multisensor capacitance probes: Laboratory calibration. Soil Sci. Soc. Am. J. 61:1576–1585.

Robinson, D.A., C.M.K. Gardner, J. Evans, J.D. Cooper, M.G. Hodnett, and J.P. Bell. 1998. The dielectric calibration of capacitance probes for soil hydrology using an oscillation frequency response model. Hydrol. Earth Sys. Sci. 2:111–120.

Robinson, D.A., S.B. Jones, J.M. Wraith, D. Or, and S.P. Friedman. 2003. A review of advances in dielectric and electrical conductivity measurement in soils using time domain reflectometry. Vadose Zone J. 2:444–475.

Saarenketo, T. 1998. Electrical properties of water in clay and silty soils. J. Appl. Geophys. 40:73–88.

Sihvola, A. 1999. Electromagnetic mixing formulas and applications. IEE Electromagnetic Waves Series No. 47. Inst. of Electrical Eng., Stevenage, UK.

Topp, G.C., J.L. Davis, and A.P. Annan. 1980. Electromagnetic determination of soil water content: Measurements in coaxial transmission lines. Water Resour. Res. 16:574–582.

Von Hippel, A.R. 1954a. Dielectrics and waves. John Wiley & Sons, New York.

Von Hippel, A.R. 1954b. Dielectric materials and applications. John Wiley & Sons, New York.